Structural optimization strategies for simple and integrally stiffened plates and shells

S.M.B. Afonso
Departamento de Engenharia Civil, Universidade Federal de Pernambuco, Recife PE, Brazil, and
J. Sienz and F. Belblidia
ADOPT Research Group, School of Engineering, University of Wales, Swansea, UK

Received February 2004
Revised December 2004
Accepted January 2005

Abstract

Purpose – Shells are widely used structural systems in engineering practice. These structures have been used in the civil, automobile and aerospace industries. Many shells are designed using the finite element analysis through the conventional and costly trial and error scheme. As a more efficient alternative, optimization procedures can be used to design economic and safe structures.

Design/methodology/approach – This paper presents developments, integration and applications of reliable and efficient computational tools for the structural optimization of variable thickness plates and free-form shells. Topology, sizing and shape optimization procedures are considered here. They are applied first as isolated subjects. Then these tools are combined to form a robust and reliable fully integrated design optimization tool to obtain optimum designs. The unique feature is the application of a flexible integrally stiffened plate and shell formulation to the design of stiffened plates and shells.

Findings – This work showed the use of different optimization strategies to obtain an optimal design for plates and shells. Both topology optimization (TO) and structural shape optimization procedures were considered. These two optimization applications, as separate procedures produce new designs with a great improvement when compared to the initial designs. However, the combination of stiffening TO and sizing optimization using integrally stiffened shells appears as a more attractive tool to be used. This was illustrated with several examples.

Originality/value – This work represents a novel approach to the design of optimally stiffened shells and overcomes the drawbacks of both topology optimization and structural shape optimization procedures when applied individually. Furthermore, the unique use of integrally stiffened shell elements for optimization, unlike conventional shell-stiffening optimization techniques, provided a general and extremely flexible tool.

Keywords Optimization techniques, Shell structures, Stiffness matrices, Plate structures

Paper type Research paper

1. Introduction

Shells are widely used structural systems in engineering practice. These structures have been used in the civil, automobile and aerospace industries. Many shells are designed using the finite element (FE) analysis through the conventional and costly

The authors acknowledge the financial support given by the Brazilian agencies CNPq, CAPES, FACEPE, FINEP and the British funding agency EPSRC for the execution of the present work.

Engineering Computations: International Journal for Computer-Aided Engineering and Software
Vol. 22 No. 4, 2005
pp. 429-452

0264-4401
DOI 10.1108/02644400510598769

trial and error scheme. As a more efficient alternative, optimization procedures can be used to design economic and safe structures.

In this context, topology optimization (TO) and conventional structural shape optimization (SSO) have been largely used in the literature and it has been the main research focus of the authors in the last decade (Afonso, 1995; Belblidia, 1999; Belblidia *et al.*, 1999, 2001; Belblidia and Hinton, 2002; Belblidia and Bulman, 2002; Falco *et al.*, 2004; Gea and Luo, 1999; Luo and Gea, 1998; Maute and Ramm, 1997).

The conventional SSO procedure enables both shape and sizing optimization to be conducted. Although both optimization applications facilitated a great improvement in the emergence of new designs, they are still limited by the fact that a suitable topology must be assumed initially.

Interest in stiffened plates and shell structures has been widespread in recent years due to economic and structural benefits. It is well known that a stiffened layout can be obtained considering both conventional sizing and also the TO procedure (Afonso and Antonino, 1998; Bendsøe and Kikuchi, 1988; Cheng and Olhoff, 1981; Gea and Luo, 1999; Luo and Gea, 1998; Maute and Ramm, 1997; Soto and Dìaz, 1993; Tenek and Hagiwara, 1994). However, the thickness distribution obtained in most of the cases is not ideal in terms of practical aspects such as ease of production, aesthetics, etc. These aspects motivate the authors for the integration of standard algorithms for TO and sizing optimization into a unique design tool.

In this work, the process of TO optimization, and sizing structural optimization are combined into a fully integrated design optimization tool, FIDO, in order to produce a reliable design of the shell. The FIDO process is conducted applying different TO procedures to evolve stiffeners on the shell, the sizes of which will be optimized. In order to get a stiffener like topology, the volume fraction for TO has to be set low otherwise the topology results will be stiffened regions instead of stiffeners or a skeleton-like topology. In this case, SSO could be applied to optimize the shape of the stiffened regions (Belblidia, 1999).

The integrated procedure considered here involves two stages. First, TO is used to determine optimal stiffening zones. A prescribed volume is chosen as an equality constraint and the objective is to find the stiffest plate/shell structure subject to a given loading, to boundary conditions and to material properties. In the second stage, stiffening zones are extracted from the optimal topology and a set of centre lines of equivalent, stiffening Timoshenko beams are selected. A sizing optimization procedure is then used to optimize the stiffener dimensions.

The sizing optimization procedure is conducted using a conventional SSO algorithm, which efficiently combines several tools such as geometric modelling, mesh generation, structural analysis, sensitivities and mathematical programming algorithms. The nine-noded degenerated Huang-Hinton element (Huang and Hinton, 1986) is used to carry out the FE analysis. When applied to stiffened structures the stiffened shell analysis is based on an appropriate integration of Ahmad degenerated shell elements and the three-noded isoparametric beam element. This FE implementation is based on the work of Bettess and co-authors (Chipalo *et al.*, 1994; Thompson, 1989). It allows any number of stiffeners to be arbitrarily located in the shell. The shell discretization is therefore independent of the stiffener layout and the inclusion of the stiffeners does not add to the overall degrees of freedom of the problem. Others, see for instance Lagaros *et al.*, 2004, rely on the conventional stiffener

arrangements that need to coincide with the shell nodal points. This could lead to an over constrained optimization problem.

In the FIDO process, the TO stage can be carried out by means of three major techniques. They are the homogenization/optimality criteria (Bendsøe and Sigmund, 2003; Rozvany *et al.*, 1992; Suzuki and Kikuchi, 1991; Zhou and Rozvany, 1991), the evolutionary methods (Baumgartner *et al.*, 1992; Xie and Steven, 1997) and the hybrid methods (Belblidia and Bulman, 2002; Bulman and Hinton, 1999; Paley *et al.*, 1996). A different classification of these methods may be found in Rozvany's (2000) work. Here, we concentrate on the homogenization and the hybrid methods. Both schemes may be based on the artificial material model or SIMP method (Rozvany *et al.*, 1992; Zhou and Rozvany, 1991). Other common aspects involved are the iterative improvement schemes used and the constraint satisfaction strategy. The updating scheme considered in the homogenization approach is based on the resizing algorithm of Bendsøe and Kikuchi (Bendsøe and Sigmund, 2003; Suzuki and Kikuchi, 1991).

The hybrid algorithm considered here is the constrained adaptive topology optimization (CATO) (Bulman and Hinton, 1999), which updates the density parameters for each element within a given domain using a volume preserving scheme which may change during the interactive process. CATO also automatically satisfies the volume fraction constraint at all stages of the iterative improvement scheme, thereby ensuring that all designs produced are valid designs unlike with most evolutionary methods, in which only the final design is valid.

In the TO procedures investigated here two distinguished layer models are used:

(1) a single layer model which consists of a single layer of artificial material which allows the introduction of holes in the shell; and

(2) a three-layer model which consists of three layers with the inner layer always solid and the outer layers consisting of artificial material.

This allows to introduce stiffening zones which are concentric to the mid-surface of the shell (Belblidia, 1999; Belblidia *et al.*, 2001). In the FIDO procedure the three-layer model is considered.

This work presents some of the aspects regarding the procedures mentioned above. It portrays some strategies that have been applied by the authors to obtain optimal plates and shells designs. In the following section, the shell elements and models are briefly described. Then the mathematical formulation for solving the structural optimization problem is presented. In the subsequent sections the main aspects of the three optimization procedures considered in this work are discussed. Some illustrative examples are presented in each of the sections. Finally, the main conclusions of this work are drawn.

2. Shell models

Two different shell elements are considered in this work. The first element is the nine-noded degenerated Huang-Hinton shell element (Huang and Hinton, 1986). It is used in the SSO procedure for shells without stiffeners and also in the TO procedure. The one-layer and three-layer models (Figure 1) can be applied in this case. For the stiffened shell analysis the eight-noded Ahmad shell type element (Ahmad, 1969) is considered. The shell models used are briefly described next.

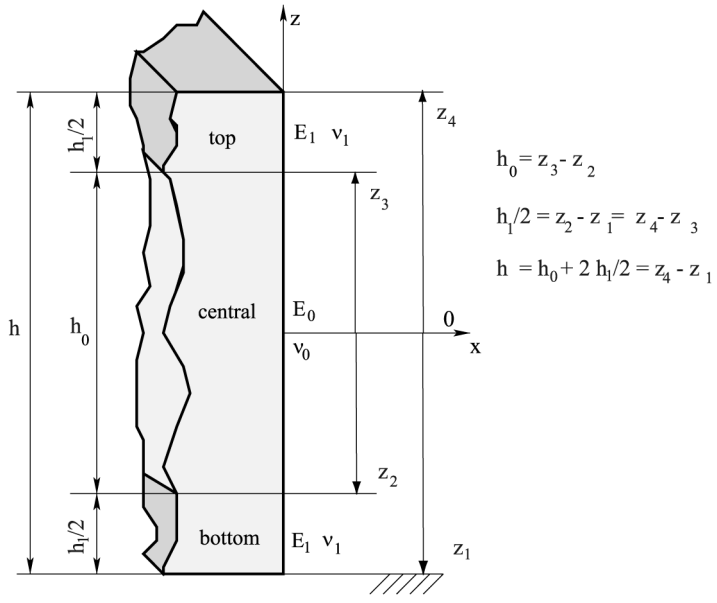

Figure 1.
Three-layered model

2.1 Layered FE shell model

We first briefly describe a layered shell model, which is used in TO. Details concerning to element geometry and displacement field can be found elsewhere (Ahmad, 1969; Huang and Hinton, 1986; Zienkiewicz and Taylor, 2000).

For a given volume V, the strain energy (SE) of a degenerated shell element (multi-layered through-thickness form) is expressed as:

$$\mathscr{U} = \frac{1}{2}\left[\int_A \varepsilon_{\mathrm{m}}^{\mathrm{T}}\mathbf{D}_{\mathrm{m}}\,\varepsilon_{\mathrm{m}}\,\mathrm{d}A + \int_A \varepsilon_{\mathrm{mb}}^{\mathrm{T}}\mathbf{D}_{\mathrm{mb}}\varepsilon_{\mathrm{mb}}\,\mathrm{d}A + \int_A \varepsilon_{\mathrm{b}}^{\mathrm{T}}\mathbf{D}_{\mathrm{b}}\varepsilon_{\mathrm{b}}\,\mathrm{d}A + \int_A \varepsilon_{\mathrm{s}}^{\mathrm{T}}\mathbf{D}_{\mathrm{s}}\varepsilon_{\mathrm{s}}\,\mathrm{d}A\right] \tag{1}$$

where ε_{m}, $\varepsilon_{\mathrm{mb}}$, ε_{b} and ε_{s} are the membrane, membrane/bending, bending, and shear generalized strains, respectively. The rigidity matrices have the following form for a multi-layered shell of thickness h with several layers:

$$\mathbf{D}_{\mathrm{m}} = \int_z \mathbf{C}_{\mathrm{p}}\,\mathrm{d}z \quad \mathbf{D}_{\mathrm{mb}} = \int_z z\mathbf{C}_{\mathrm{p}}\,\mathrm{d}z \quad \mathbf{D}_{\mathrm{b}} = \int_z z^2\mathbf{C}_{\mathrm{p}}\,\mathrm{d}z \quad \mathbf{D}_{\mathrm{s}} = \frac{1}{\alpha}\int_z \mathbf{C}_{\mathrm{s}}\,\mathrm{d}z \tag{2a}$$

in which α is the shear modification factor, and where for an isotopic material of elastic modulus E and Poisson's ratio ν:

$$\mathbf{C}_{\mathrm{p}} = \frac{E}{1-\nu^2}\begin{bmatrix} 1 & \nu & 0 \\ \nu & 1 & 0 \\ 0 & 0 & (1-\nu)/2 \end{bmatrix} \text{ and } \mathbf{C}_{\mathrm{s}} = \frac{E}{2(1+\nu)}\begin{bmatrix} 1 & 0 \\ 0 & 1 \end{bmatrix}. \tag{2b}$$

For both single- and three-layered shell models considered here $\mathbf{D}_{\mathrm{mb}} = 0$.

The three-layered model considered here is shown in Figure 1. The central layer is always taken as being solid, whereas the upper and lower layers may represent a porous material. This is called the stiffening model. For this model, the rigidities have the form:

$$\begin{aligned} &\mathbf{D}_{\mathrm{m}} = h_0\mathbf{C}_{\mathrm{p0}} + (h-h_0)\mathbf{C}_{\mathrm{p1}} \quad \mathbf{D}_{\mathrm{b}} = \frac{h_0^3}{12}\mathbf{C}_{\mathrm{p0}} + \frac{\left(h^3 - h_0^3\right)}{12}\mathbf{C}_{\mathrm{p1}} \\ &\mathbf{D}_{\mathrm{s}} = \frac{1}{\alpha}(h_0\mathbf{C}_{\mathrm{s0}} + h_1\mathbf{C}_{\mathrm{s1}}) \end{aligned} \tag{3}$$

In the above equations, h is the total thickness of the shell, the subscript "0" refers to the central layer and subscript "1" refers to the top and bottom layers, respectively.

The above formulation may be used as a basis for developing a degenerated shell FE. In the present work we have selected the Huang-Hinton nine-noded isoparametric element (Huang and Hinton, 1986) which avoids shear and membrane locking and mechanisms, and gives good overall behaviour.

2.2 Stiffened shell formulation

In order to perform the optimization of stiffened shells, beam stiffeners are incorporated in the conventional degenerated shell formulation (Afonso and Antonino, 1999; Huang and Hinton, 1986).

In this work the stiffened shell analysis is based on an appropriate integration of the eight-noded Ahmad shell element (Ahmad, 1969) and the three-noded isoparametric beam element (Figure 2). This FE implementation is due to the work of Bettess and co-authors (Chipalo *et al.*, 1994; Thompson, 1989). The existing advantages inherent to this formulation over the conventional approaches are of particular benefit for optimization (Afonso and Antonino, 1999).

For prescribed natural coordinates ξ_0, η_0, ζ_0 it is assumed that the beam cross-section has the direction z' which coincides with the direction of the corresponding shell normal (Figure 2). This assumption allows us to express the beam axis displacement fields as:

$$\mathbf{u}_{\mathrm{s}}(\chi) = \mathbf{u}(\xi_0, \eta_0, \zeta = 0) = \begin{pmatrix} u_{\mathrm{s}} \\ v_{\mathrm{s}} \\ w_{\mathrm{s}} \end{pmatrix} = \begin{pmatrix} u' + y'\gamma' - z'\beta' \\ v' + z'\gamma' \\ w' - y'\alpha' \end{pmatrix} \tag{4}$$

where χ is a local coordinate along the stiffener curvilinear axis shown in Figure 2, u_{s}, v_{s} and w_{s} are the displacements of any point in the x, y and z directions and u, v and w are the local translations at $\mathbf{x}(\xi_0, \eta_0, \zeta = 0)$ in the direction of the x, y and z directions, respectively.

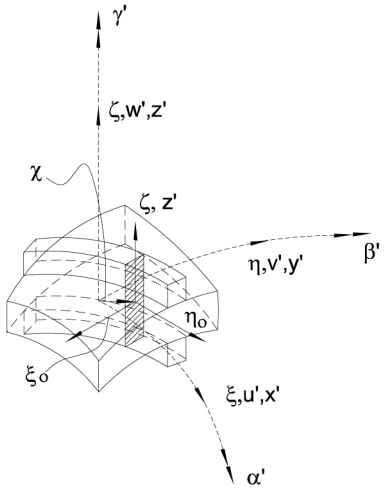

Figure 2.
Geometry of a stiffened shell element

For stiffener i of a typical element e, the stiffness matrix may be expressed as:

$$\mathbf{k}_i^e = \int_{S_i} \mathbf{B}_{\mathrm{st}_i}^{\mathrm{T}} \mathbf{D}_{\mathrm{st}} \mathbf{B}_{\mathrm{st}_i} \, \mathrm{d}s \quad = \int_{-1}^{1} \mathbf{B}_{\mathrm{st}_i}^{\mathrm{T}} \mathbf{D}_{\mathrm{st}} \mathbf{B}_{\mathrm{st}_i} s_{,\chi} \, \mathrm{d}\chi \tag{5}$$

where

$$s_{,\chi} = \sqrt{\left(x_{,\chi}^2 + y_{,\chi}^2 + z_{,\chi}^2\right)}. \tag{6}$$

The complete stiffness formulation for a stiffener shell element is given by the sum of the stiffness matrix contributions of the individual stiffeners and the host shell element. Thus for a host shell element containing m arbitrarily placed stiffeners, the total stiffness is computed as follows:

$$\mathbf{k}_{\mathrm{total}} = \underbrace{\int_{-1}^{1}\int_{-1}^{1} \mathbf{B}^T \mathbf{D} \mathbf{B} \|\mathbf{J}\| \mathrm{d}\xi \, \mathrm{d}\eta}_{\text{host shell element}} + \sum_{i=1}^{m} \underbrace{\left(\int_{-1}^{1} \mathbf{B}_{\mathrm{st}_i}^T \mathbf{D}_{\mathrm{st}} \mathbf{B}_{\mathrm{st}_i} s_{,\chi} \, \mathrm{d}\chi \right)}_{\text{integral stiffeners}}. \tag{7}$$

3. Structural optimisation

The structural optimization problem can be expressed as a relation, which involves the objective function and the constraint functions. It can be expressed mathematically as:

$$\text{minimize (or maximize)}: \quad F(\mathbf{s}) \tag{8}$$

subject to

$$
\begin{aligned}
& g_i(\mathbf{s}) \leq 0 \quad i = 1, \ldots, m \\
& h_j(\mathbf{s}) = 0 \quad j = 1, \ldots, \ell \\
& s_k^{\ell} \leq s_k \leq s_k^{\mathrm{u}} \quad k = 1, \ldots, n_{\mathrm{dv}}.
\end{aligned} \tag{9}
$$

Here $\mathbf{s}$ is the vector of design variables, $F(\mathbf{s})$ the objective function, $g_i(\mathbf{s})$ and $h_j(\mathbf{s})$ are the constraint functions. Finally, s_k^{ℓ} and s_k^{u} represent the lower and upper limits of a typical design variable s_k. m is the number of inequality constraints, ℓ the number of equality constraints and n_{dv} the number of design variables.

4. Topology optimisation

In this work TO is conducted by both homogenization and hybrid methods. The hybrid method considered is CATO (Belblidia and Bulman, 2002; Bulman and Hinton, 1999). In both procedures the same type of material is used which is described below.

4.1 Material model for topology optimisation

Adopting this model, the constitutive matrices are written as:

$$
\mathbf{C}_{\mathrm{p}}^{h} = \chi(x)\mathbf{C}_{\mathrm{p}} \text{ and } \mathbf{C}_{\mathrm{s}}^{h} = \chi(x)\mathbf{C}_{\mathrm{s}} \tag{10}
$$

where $\chi(x)$ is a discrete function defined at each point x over the whole domain Ω, and which has the form:

$$
\chi(x) = \begin{cases} 1 & \text{if } x \in \Omega_{\mathrm{s}} \quad \text{material} \\ 0 & \text{if } x \in \Omega\ \Omega_{\mathrm{s}} \quad \text{no material.} \end{cases} \tag{11}
$$

The discrete form of function $\chi(\mathbf{x})$ causes some solution difficulties, which can be overcome by replacing χ by a continuous function ξ, where $0 \leq \xi(\mathbf{x}) \leq 1$ and $\mathbf{x} \in V$. It is desired to relate ξ to some geometric parameters in order to create some sort of micro-structure representation. If we assume the micro-structure as a cellular body consisting of unit cells with square hole of side length a where $0 \leq a \leq 1$, then the material content of a cell can be expressed as:

$$
\xi(x) = 1 - a^2(x). \tag{12}
$$

The rigidity matrices used here in the stiffening layers will finally be written as:

$$
\mathbf{C}_{\mathrm{p}}^{h} = \xi(x)^{\gamma}\mathbf{C}_{\mathrm{p}} \text{ and } \mathbf{C}_{\mathrm{s}}^{h} = \xi(x)^{\gamma}\mathbf{C}_{\mathrm{s}} \tag{13}
$$

in which γ is a penalizing parameter considered to suppress the porous areas as suggested by Zhou and Rozvany (1991). For the three-layer FE model described, the membrane, bending and shear rigidities matrices are obtained from equation (3) applying to the top and bottom layer the corrections indicated in equation (13).

Note that although we have assumed a micro-cellular material with a square hole size a, we have approximated the resulting material behaviour as though it was isotropic (with a scaling factor) rather than truly orthotropic. Truly orthotropic behaviour could be considered by including an additional design variable θ for the orientation of the material model. In the present work, there is no dependency on

the orientation of the square hole in the artificial material model unlike it is the case for the more conventional homogenized model.

In the examples presented later, the normalized value $\mathscr{U}/\mathscr{U}_{\text{initial}}$ is used to show the variation of the strain energy. Because we are dealing with the artificial material model in a penalized form, the resulting strain energy value is therefore not exact (Hassani and Hinton, 1999).

4.2 Homogenization procedure

If we parameterize the stiffener density $\varrho_e = 1 - a$ in each element e our problem is essentially one of determining the set of ϱ, which minimize the strain energy of the shell for a total, user specified volume fraction of stiffened material.

4.2.1 Basic algorithm. The full TO is summarized in the following steps.

(1) Read problem data including the mesh data, the boundary and the loading conditions, the material properties, the definition of the design and the non-design domains, the target volume and various solution parameters.

(2) Before starting the topology optimization loop, initialize the density parameters ϱ_e for each element and evaluate the rigidity matrices. Set the iteration parameter $k = 0$.

(3) Increment the iteration number k by 1.

(4) Perform the FE analysis for the current rigidity matrices.

(5) Resize the density parameter ϱ_e within each element based on a resizing algorithm to be described.

(6) Check the optimization termination criteria: if this is satisfied then output the optimal density parameters and terminate the solution. Otherwise go to step 3.

Next, we will consider the necessary optimality conditions, the resizing algorithm and some computational implementation issues.

4.2.2 Optimality criteria and resizing algorithm. The TO can be stated as minimize the total strain energy $\mathscr{U}$ with a specified volume V_{S} as a constraint (equality or inequality). The material density parameters $\varrho = (\rho_1, \rho_2, \ldots, \rho_{\text{nel}})^{\text{T}}$ are the design variables of the problem and nel is the number of FEs. Considering the above objective function and constraint, the necessary optimality conditions for the material density parameters ϱ are a subset of the stationary conditions of the Lagrangian function $\mathscr{L}$ in the discretized domain:

$$\begin{aligned}\mathscr{L}(\rho) = \sum_{e=1}^{\text{nel}} \mathscr{U}_e + \Lambda\left(\sum_{e=1}^{\text{nel}} \int_{V_e} (2\varrho_e - \varrho_e^2)\mathrm{d}V - V_{\text{s}}^0\right) \\ + \sum_{e=1}^{\text{nel}} \left(\int_{V_e} \lambda_{\varrho_e}^{+}(\varrho_e - 1)\mathrm{d}V - \int_{V_e} \lambda_{\varrho_e}^{-}\varrho_e \,\mathrm{d}V\right)\end{aligned} \tag{14}$$

where Λ, $\lambda_{\varrho_e}^{+} = \left[\lambda_{\varrho_1}^{+}, \lambda_{\varrho_2}^{+}, \ldots, \lambda_{\varrho_{\text{nel}}}^{+}\right]$ and $\lambda_{\varrho_e}^{-} = \left[\lambda_{\varrho_1}^{-}, \lambda_{\varrho_2}^{-}, \ldots, \lambda_{\varrho_{\text{nel}}}^{-}\right]$ are positive Lagrangian multipliers and $\mathscr{U}_e$ is the strain energy of the shell element e. For uniform FE meshes, as used for all the examples here, the stationary conditions of the Lagrangian function for the material density ϱ_e are:

$$\frac{\partial \mathscr{L}}{\partial \varrho_e} = \frac{\partial \mathscr{U}}{\partial \varrho_e} + 2\Lambda(1 - \varrho_e) + \lambda^+_{\varrho_e} - \lambda^-_{\varrho_e} = 0, \quad e = 1, \ldots, \text{nel} \tag{15}$$

or

$$-\frac{\partial \mathscr{U}}{\partial \varrho_e} = 2\Lambda(1 - \varrho_e) + \lambda^+_{\varrho_e} - \lambda^-_{\varrho_e}, \quad e = 1, \ldots, \text{nel} \tag{16}$$

with the switching conditions

$$\lambda^-_{\varrho_e} \geq 0, \quad \lambda^+_{\varrho_e} \geq 0, \quad \lambda^-_{\varrho_e}\varrho_e = 0, \quad \lambda^+_{\varrho_e}(\varrho_e - 1) = 0, \quad e = 1, \ldots, \text{nel}. \tag{17}$$

For intermediate values of the density parameter, $0 \leq \varrho_e \leq 1$, when the side constraint is inactive, then $\lambda^-_{\varrho_e} = \lambda^+_{\varrho_e} = 0$, and the necessary condition can be rewritten as:

$$\frac{1}{-2\Lambda(1 - \varrho_e)}\frac{\partial \mathscr{U}}{\partial \varrho_e} = 1, \quad e = 1, \ldots, \text{nel}. \tag{18}$$

In short, equation (18) can be written as:

$$-B_{\rho_e} = 1 \tag{19}$$

in which

$$B_{\rho_e} = \frac{1}{2\Lambda(1 - \varrho_e)}\frac{\partial \mathscr{U}}{\partial \varrho_e}, \quad e = 1, \ldots, \text{nel}. \tag{20}$$

However, if for a particular iteraction k, the design variable has decreased, i.e. $\varrho^k_e \leq 1$ and therefore the upper limit is not active, yielding $\lambda^+_{\varrho_e} = 0$, from equations (16) and (17) it follows that $B^k_{\varrho_e} \geq 1$. On the other hand, for increasing ϱ^k_e we will get $B^k_{\varrho_e} \leq 1$. The above argument provides the information required in the resizing algorithm, devised in the following form as described by Bendsøe and Sigmund (2003):

$$\varrho^{k+1}_e = \begin{cases} \text{MAX}_0 & \text{if } \varrho^k_e\left(B^k_{\varrho_e}\right)^\eta \leq \text{MAX}_0 \\ \varrho^k_e\left(B^k_{\varrho_e}\right)^\eta & \text{if } \text{MAX}_0 \leq \varrho^k_e\left(B^k_{\varrho_e}\right)^\eta \leq \text{MIN}_1 \\ \text{MIN}_1 & \text{if } \text{MIN}_1 \leq \varrho^k_e\left(B^k_{\varrho_e}\right)^\eta \end{cases} \tag{21}$$

in which $\text{MAX}_j = \max\{(1 - \omega)\varrho^k_e, j\}$, $\text{MIN}_j = \min\{(1 + \omega)\varrho^k_e, j\}$. η is a tuning parameter and ω is a move limit. The superscript k means the kth iteration. $B^k_{\varrho_e}$ is the value of B_{ϱ_e} at iteration k.

4.2.3 Updating procedure and termination criteria. The resizing procedure described in the previous section is implemented as follows.

(1) Using a given volume fraction, calculate the initial value for the design variables which are the material density parameters ϱ_e
(2) Calculate the displacements $\mathbf{u}$ using the artificial material model
(3) Calculate the strain energy $\mathscr{U}$ and its derivatives
(4) Estimate Lagrangian multiplier Λ using (18)
(5) Update design variables

(5a) Update material density parameters ϱ_e using (21)

(5b) Check whether new material density parameters ϱ_e satisfy the volume constraint

(5c) If yes, go to step 6. Otherwise, use bisection method until the volume constraint is satisfied and then if it is satisfied, go to step 6

(6) If the termination criteria is satisfied, stop. Otherwise, repeat steps 2-5

In step 6, several termination criteria can be used in TO. Three eligible termination criteria used for TO here can be summarized as follows:

(1) *Maximum number of iterations.* A fixed number of iterations can be provided by the user. The TO will continue for the given number of iterations.

(2) *Decrease percentage of strain energy.* If the strain energy of the structure reaches a given strain energy value, i.e. $\mathscr{U}^k \leq \mathscr{U}^0$, the iterative process will stop.

(3) *Volume changes.* If the sum of volume changes over all elements from one iteration to the next is less than a specified value, then iterating will stop.

4.3 CATO procedure

The aim of CATO is to update the density parameters for each element within a given domain using a volume preserving scheme, which may change during the iterative improvement. CATO also automatically satisfies the volume fraction constraint at all stages of the improvement scheme, thereby ensuring that all designs produced are valid designs unlike with most E-methods, in which only the final design is valid.

4.3.1 Basic algorithm. The CATO algorithm has the following steps.

(1) Set up the data regarding the design domain, the optimization and the FE model. Set the iteration counter $k = 1$.

(2) For the desired volume fraction, V_{frac}, initialize the material density parameters a_e^k for each element according to the expressions.

$$a_e^k = \begin{cases} 0 & \text{if non-design domain} \\ (1 - V_{\text{frac}})^{1/2} & \text{if design} \\ a_{\text{pr}} & \text{if prescribed} \end{cases}$$

Also, calculate the desired volume of the system V_{des} using

$$V_{\text{des}} = V_{\text{frac}} * \sum_{e=1}^{\text{nel}} v_e,$$

where nel is the number of elements present in the model and v_e is the volume of element e.

(3) Evaluate the appropriate constitutive properties using an artificial material model considering the current a_e^k values.

(4) Perform the FE analysis.

(5) Order the elements according to their strain energy density values.

(6) From a specified volume preserving relationship $\Delta a_e^k(f_e)$ evaluate the change of the density parameters Δa_e^k for each element and update the density parameter so that $a_e^{k+1} = a_e^k + \Delta a_e^k$.

(7) Given the new density parameters a_e^{k+1}, evaluate the overall structural volume of the system V_{sys}.

(8) Check the requirement that $\left|\frac{V_{\text{sys}}}{V_{\text{des}}} - 1\right| < V_{\text{tol}}$. If this condition is not satisfied, adjust a_e^{k+1} proportionately to obtain $V_{\text{sys}} = V_{\text{des}}$ and go to step 7.

(9) If some convergence criterion is met continue with step 10, otherwise set $k = k + 1$ and return to step 3.

(10) Post-process the results prior to visualization and then terminate the solution.

4.3.2 CATO material updating scheme. The CATO algorithm uses an incremental relationship $\Delta a_e(f_e)$ to adjust the elemental material parameter a_e according to the element strain energy density value f_e. A special feature of this relationship is that it is chosen so as to preserve the total volume of the structure during the iterative optimization process. The details of such an updating scheme can be found elsewhere (Bulman and Hinton, 1999). Here, we will briefly explain the procedure. Figure 3 shows an example of this relationship at two stages of the scheme. The function is composed of a curve of the form $y = n^{p_{\text{cur}}}$ (n and p_{cur} are described later), which join at the x-axis.

The change in the density parameter Δa_e^k for element e at iteration k, is shown in Figure 3 and is given by:

$$\Delta a_e^k = \alpha n_e^{p_{\text{cur}}}, \tag{22}$$

where

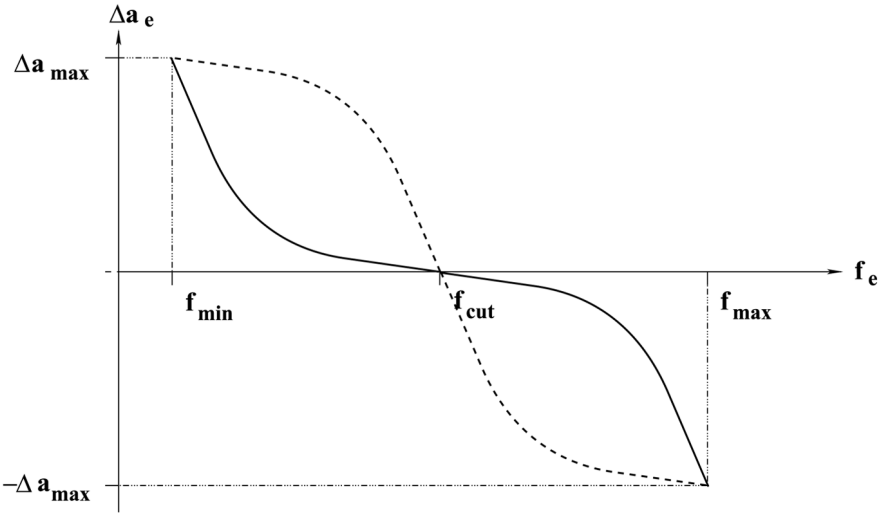

Figure 3.
Example of the relationship $\Delta a_e(f_e)$ at an early stage of the iterative scheme (solid line), and at an intermediate stage (dashed line)

$$\alpha = -\frac{(f_e - f_{\text{cut}})}{|f_e - f_{\text{cut}}|}, \quad n_e = (f_e - f_{\text{cut}})/r, \quad p_{\text{cur}} = p_{\text{init}} - ((k - 1.0) * \text{iter}), \tag{23}$$

and r is defined as:

$$r = \begin{cases} f_{\max} - f_{\text{cut}} & \text{if } f_e > f_{\text{cut}} \\ f_{\min} - f_{\text{cut}} & \text{if } f_e \leq f_{\text{cut}}. \end{cases} \tag{24}$$

where p_{init} is the initial curve exponent parameter, iter controls how the curve adapts through the iterative scheme, and niter is the maximum number of iterations specified by the user.

After calculating the density parameters a_e^k for all elements, the volume of the new system is evaluated to check the volume equality constraint:

$$\left| \frac{V_{\text{sys}}}{V_{\text{des}}} - 1 \right| < v_{\text{tol}}, \tag{25}$$

where V_{sys} is the current system volume, V_{des} is the desired system volume and V_{tol} is some allowable tolerance on the volume constraint, typically less than 1 per cent.

If it is satisfied, then the algorithm can proceed to the next iteration. However, if equation (25) is not satisfied then the volume error for each element is calculated as:

$$V_{\text{err}} = \frac{V_{\text{sys}} - V_{\text{des}}}{\text{nel}} \tag{26}$$

and the new density parameter a_{i+1}^e for each element is calculated as:

$$a_e^{k+1} = a_e^k + V_{\text{err}}. \tag{27}$$

4.3.3 Convergence and termination criteria. Three termination criteria are used in the CATO process. If one of them is satisfied, the TO iteration is terminated. These criteria are:

(1) the number of iterations exceeds a number specified by the user;

(2) the change in strain energy between any three successive iterations is below a given tolerance; and

(3) there is an increase in the strain energy in three successive iterations.

After convergence some post-processing of the results for further analysis or optimization can be carried out. This can include thresholding, boundary fitting and parameterization.

5. TO examples

The procedures described before to obtain optimal topologies are now illustrated for several plates and shell problems.

In the first set of examples comparison tests are conducted on some plate examples using both homogenization and CATO procedures. In this case, a three-layered artificial material is considered and the parameters used for the CATO algorithm are: volume fraction $V_{\text{f}} = 50$ per cent, artificial material exponent $\gamma = 3$, maximum

incremental density parameter $\Delta a_{\max} = 0.05$, the initial curve exponent parameter $p_{\text{init}} = 1.5$, and the interative advancing parameter iter is 0.025. A maximum of 200 iterations is specified with a convergence tolerance in the change of the strain energy of 1 per cent. For homogenization the equivalent set a data is used. For each example, the optimum topology design is given for CATO and the homogenization technique. All units are assumed to be consistent.

In the subsequent set of examples, CATO is applied to optimize shell structures using a single- and a three-layered material model. The parameters used for the CATO algorithm are: volume fraction $V_{\text{f}} = 35$ per cent, artificial material exponent $\gamma = 5$, maximum incremental density parameter $\Delta a_{\max} = 0.05$, the initial curve exponent parameter $p_{\text{init}} = 3$, and the iterative advancing parameter iter is 0.025. A maximum of 200 iterations is assumed with a convergence tolerance in the change of the strain energy of 1 per cent.

5.1 Plate bending problems: comparing homogenization and CATO

We now consider some plates subjected to a vertical central point load. In these examples, the problem data are: elastic modulus $E = 10.92 \times 10^5$, Poisson's ratio $\nu = 0.3$, load magnitude $F = 100$, and the plate thickness $h = 0.1$.

In all examples only a symmetric quadrant of the plate is analysed, however, the topology image shows the result for the whole plate.

Simply supported square plate. The stiffening topology for all four edges simply supported and centrally loaded square plate is optimized.

A structured FE mesh consisting of 625 (25×25) quadrilateral nine-noded shell elements is used to idealize the plate quadrant, and the plate side length is $a = 10$. In this case a maximum of 200 iterations is used for the optimization.

Figure 4 shows the optimal stiffening topology and the convergence of the normalized strain energy using homogenization (left), and CATO (right) based on the three-layered model for the centrally loaded square plate. Good agreement is found between the presented solutions, with CATO delivering a sharp image using fewer iterations.

Clamped supported circular plate. The stiffening topology for the clamped supported circular plate under central point load is to be determined. A structured FE mesh consisting of 675 quadrilateral nine-noded shell elements is used to idealize the symmetric plate quadrant. The plate radius is $r = 1$. Figure 5 shows the optimal stiffening topology and the convergence of the normalized strain energy using homogenization (left) and CATO (right) based on the three-layered model for the circular plate under central point load. As can be observed, similar results are obtained using both schemes.

5.2 Shell problems: topology studies considering different layered models and CATO

In these examples, the problem data are: elastic modulus $E = 10.92 \times 10^3$, Poisson's ratio $\nu = 0.3$, load magnitude $F = 100$, and the shell thickness $h = 0.1$. Again, only the symmetric quadrant of the shell is analysed. In all examples the topology image shows the result for the whole shell structure.

For all examples a structured FE mesh consisting of 400 (20×20) quadrilateral nine-noded shell elements is used to idealize the symmetric part of the shell considered and its projection on the xy plane is a square of side length $a = 100$. The single-layered

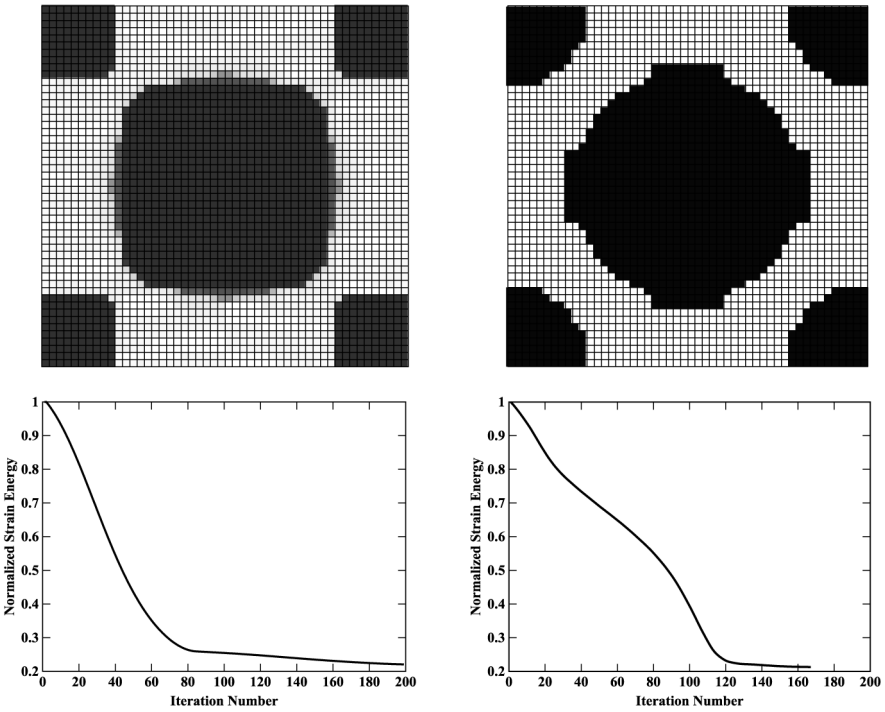

Figure 4.
Results for simply supported square plates under central point load using the three-layered model

Notes: Top: Optimal stiffening topology, Bottom: Convergence of the normalized strain energy. Left: Homogenization, Right: CATO

model shows the topology of the remaining structure. For the three-layered model the dark areas show the necessary stiffeners that are attached to the top and to the bottom surface of the solid midplane, respectively.

Cylindrical shell. Here, a half cylinder with a radius $r = 100.0$ is used to present the shell geometry. The cylindrical shell is subjected to a central point load and it is clamped at its four corners. Figure 6(a) and (b) shows the optimal topologies for the cylindrical shell using a single-layered and a three-layered model, respectively.

Elliptic parabolic (EP) shell. The shell studied here is an EP shell defined geometrically by the equation $z(x, y) = 0.57(x^2 + y^2)$. The shell is subjected to a central point load and the edges are clamped. When considering the three-layered model the central layer has a thickness $h_0 = 0.05$ and the top and bottom layers have a combined thickness of $h_1 = 0.05$. The optimum topologies obtained for the EP shell when considering the single-layer and the three-layered stiffening models are indicated in Figure 7(a) and (b), respectively. The solutions are accomplished with a 60 per cent SE reduction and 40 per cent SE reduction, respectively.

Free form shell. The shell surface is defined by a sphere of radius $r = 10$ and it is clamped at its four corners. Figure 8(a) and (b) shows the optimal topologies for the spherical shell using a single-layered and a three-layered model, respectively.

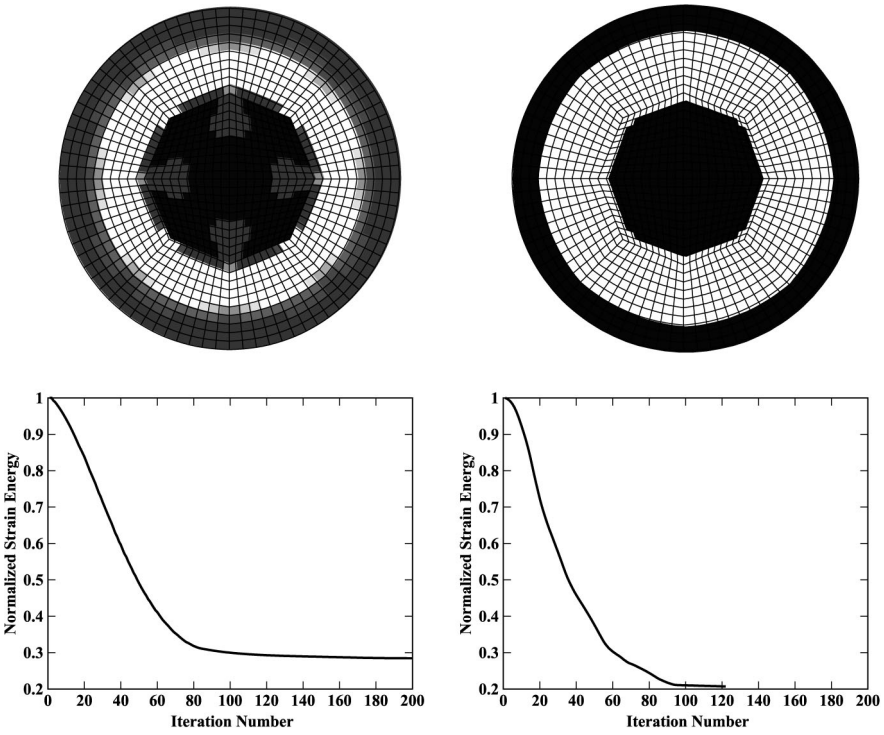

Source: Top: Optimal stiffening topology, Bottom: Convergence of the normalized strain energy, Left: Homogenization, Right: CATO

Figure 5.
Results for the clamped supported circular plate under central point load using the three-layered model

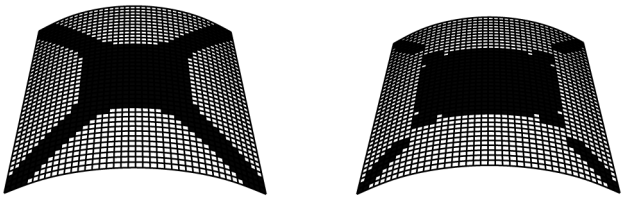

(a) **(b)**

Notes: (a) single-layer model and (b) three-layer model

Figure 6.
Cylindrical shell example – optimal topologies

For all the examples analysed here, as expected, when the single-layered stiffening model is considered all of the stiffening areas are connected to each other. However, when the three-layered stiffening model is used some stiffening areas may not be connected to each other due to the existence of the solid central layer in these structures.

6. SSO procedure

The optimum shape of shells can be found using an automatic SSO procedure in which the boundary and/or the thickness distribution of the structures is varied to achieve a desired objective satisfying certain constraints.

In the current approach, when shell structures are considered, both coordinates and thicknesses at the key points used to represent the shell geometry can be selected as design variables (Afonso, 1995; Rao, 1992). Additionally, for stiffened structures the dimensions and the positions of the stiffeners can be considered as design variables (Afonso and Antonino, 1998).

The basic algorithm for the SSO of shells is now described. The main steps presented are briefly explained and provide a general overview of the various modules involved. More detailed descriptions of each step may be found elsewhere (Afonso, 1995; Afonso and Antonino, 1998; Powell, 1978; Rao, 1992; Sienz, 1994).

(1) Define the optimization problem.

(2) Create the design model.

(3) Create FE model.

(4) Carry out the FE analysis.

(5) Evaluate sensitivities.

(6) Carry out the optimization.

If the new structure is not optimal, we continue the whole process from step 3 producing a sequence of new designs until an optimal solution is obtained.

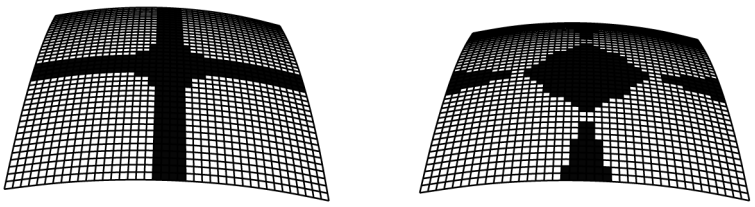

Notes: (a) single-layer model and (b) three-layer model

Figure 7.
EP shell example – optimal topologies

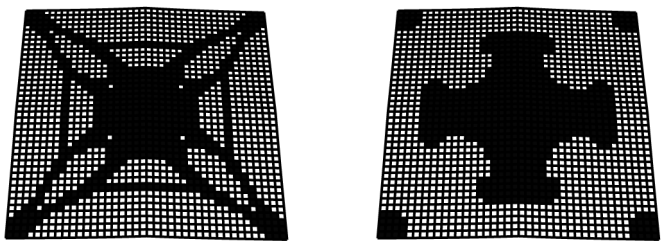

Note: (a) single-layer model and (b) three-layer model

Figure 8.
Free-form shell example – optimal topologies

7. SSO examples

7.1 Introduction

In this section, we demonstrate the application of the SSO procedure involving different types of structures.

7.2 Variable thickness square plates

A set of square plates (Figure 9) with initial thickness to span ratio h/L of 0.1 are considered. Each plate is subjected to a uniform normal pressure load of unity intensity. The following material properties are assumed in the analysis so that the results may be presented in non-dimensional form: the elastic modulus E is taken to be $10.92 \times h^{-2}$, and Poisson's ratio $\nu = 0.3$, so that the flexural rigidity $D = 1$ where $D = Eh^3/12(1 - \nu^2)$.

Two different types of boundary conditions are considered:

(1) S_h – all round hard simple support (lateral displacement $w = 0$ and tangential edge rotation $\theta = 0$; and

(2) S – all round soft simple support ($w = 0$).

The objective is to minimize the total SE with the constraint that the volume is kept constant. Only a symmetric quadrant of the plates is analysed. Figure 9 shows the patches in the symmetric quadrant and the locations of the design variables. A 10×10 mesh is used to model the symmetric quadrant. Studies (Afonso, 1995; Cheng and Olhoff, 1981) demonstrated that the results are highly dependent on the number of design variables used, but less dependent on the FE discretization.

Different thickness distributions are obtained for the various cases optimized. The optimization results are shown in Figures 10 and 11, respectively, for the soft simple support and the hard simple support boundary conditions. Table I gives the percentage reductions in the SE for the plates studied. For a particular problem, it is observed that the reductions are greater for the hard support boundary condition and when more design variables are used.

7.3 Stiffened plate

A square plate with side length $L = 2$ and four stiffeners as shown in Figure 12 is now considered. The plate is subjected to a uniform normal pressure load of unit intensity. The following material properties are assumed: elastic modulus $E = 19.92\,\mathrm{kN/m^2}$ and

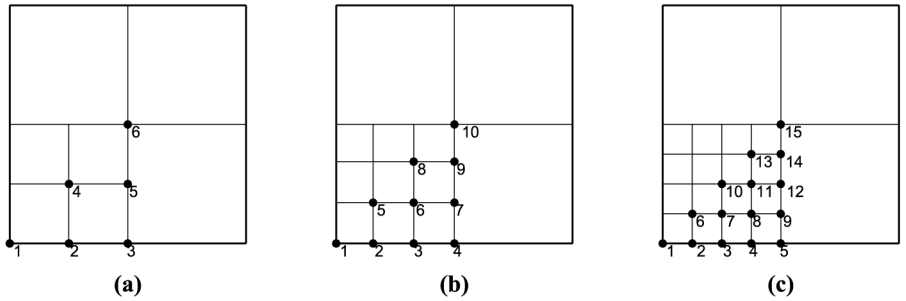

Notes: (a) 6dv, (b) 10 dv and (c) 15dv

Figure 9.
Plate example – location of the thickness design variables

(a) (b) (b)

Notes: (a) 6dv, (b) 10dv and (c) 15dv (N.B.darkest shading is thickest zone)

Figure 10.
Plate example – optimal thickness distribution for soft simple support

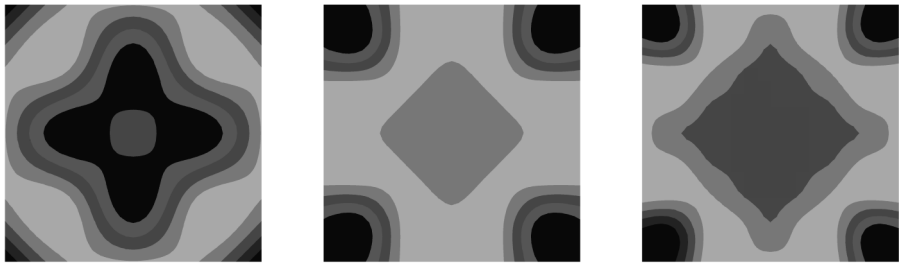

(a) (b) (c)

Notes: (a) 6dv, (b) 10dv and (c) 15dv (N.B. darkest shading is thickest zone)

Figure 11.
Plate example – optimal thickness distribution for hard simple support

ndv	6	10	15
S	30	32	34
S_h	31	38	38

Note: Percentage reduction in SE for different boundary conditions and different number of design variables

Table I.
Square plate example

Poisson's ratio $\nu = 0.30$. The whole structure is analysed using a 12×12 mesh. The horizontal edges of the plate are clamped while the vertical edges of the plate are hard simply supported.

The SE of the plate is to be minimized subject to the constraint that the initial volume remains constant. A total of eight design variables is considered. They are: plate thickness, height of three selected regions along all stiffeners (h_1, h_2, h_3 in Figure 12), the position of the horizontal stiffeners (y coordinates) and the position of the vertical stiffeners (x coordinates).

The design variable values are given in Table II. A big SE reduction of 54 per cent is obtained in this case. This is mainly due to the inclusion of three different regions (one design variable for each region) for each stiffener. This allowed more freedom during the optimization process so that the plate could be stiffened where it was vital.

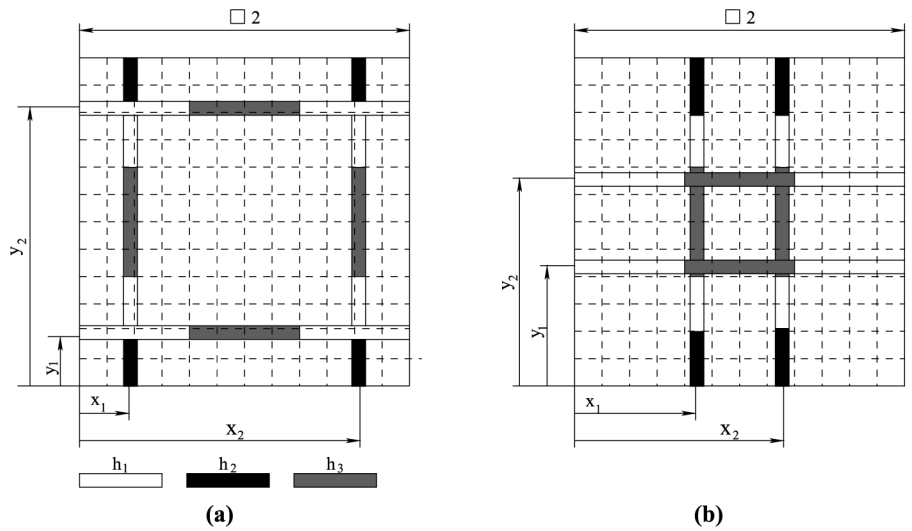

Notes: (a) initial configuration and (b) final configuration

Figure 12.
Plate with multiple stiffeners example

Description	Design variables values							
		Heights			Coordinates			
	t_p	h_1	h_2	h_3	x_1	x_2	y_1	y_2
Initial	0.12	0.40	0.40	0.40	0.30	1.70	0.30	1.70
Lower bound	0.06	0.20	0.20	0.20	0.05	1.05	0.05	1.05
Upper bound	0.224	1.00	1.00	1.00	0.95	1.95	0.95	1.95
Optimum	0.081	0.628	0.343	1.00	0.74	1.26	0.72	1.28

Table II.
Plate with multiple stiffeners – optimization results

The final position of the stiffeners is shown in Figure 12(b), which seems consistent with the plate boundary conditions.

8. Integrated optimization procedure and examples

8.1 Integration of standard algorithms

The potential of the topology and sizing optimization procedures was demonstrated in the previous sections as independent tools to obtain optimum plates and shells solutions. In this section, these procedures are combined as a unique design tool with special emphasis on a specific problem. The objective is to find the stiffest structure, subject to a given loading and to a given set material properties, which fits within a specified design space and which has a specified volume. In the integrated procedure, three main stages are involved in the determination of the optimum solutions:

(1) identification of areas in which the shell should be stiffened using TO results;

(2) definition of discrete stiffeners axes and zones of piecewise constant stiffeners variables; and

(3) evaluation of optimum stiffener dimensions using sizing optimization procedure.

8.2 Introduction to FIDO examples

The applicability of the FIDO procedure is now demonstrated for a set of examples. The procedure is initially applied to a plate. Then some shells with different geometries are considered. This involves an EP shell and a cylindrical shell. In all examples the common parameters used for the topology algorithms are: the maximum number of interactions allowed is 200 and the convergence tolerance parameters with respect to the SE is 1 per cent, Other parameters which are related to the material updating scheme of CATO are: maximum incremental density parameter $\Delta a_{\max} = 0.05$, the initial curve exponent parameter $P_{\text{init}} = 5$ and the iterative advancing parameter iter $= 0.025$. The specific parameters when using homogenization algorithms were: artificial material exponent $\gamma = 5$, tuning parameter $\eta = 0.8$, moving limit $\zeta = 0.8$, and volume constraint tolerance $\delta = 0.001$. During the procedure the following aspects are considered:

(1) The objective is the minimization of the strain energy keeping the total volume constant to $V = V_{\text{frac}}$.

(2) The maximum stiffener thickness allowed is the maximum thickness allowed for the plate/shell in the topology optimization.

(3) A three-layer model is considered in the topology optimization.

(4) The regions of maximum and minimum thickness are dictated by the topology image results. Therefore, the maximum and the minimum thickness for the stiffeners correspond to the darkest and to the brightest areas, respectively, in the topology images (the thicknesses for the stiffeners corresponding to the lighter areas are the same as the central layer thickness of the shell in the topology model).

(5) Along the stiffeners, different regions are selected guided by the topology optimization results. Each of these regions is associated with a design variable. In the present studies the design variables are the stiffener widths in these regions.

(6) All units are considered to be consistent.

(7) Only a symmetric quadrant of each plate is analysed.

(8) The meshes adopted consist of 40×40 shell elements in the topology study and 12×12 shell elements in the sizing optimization study.

8.3 Plate example

A flat roof supported by four columns and supporting a central point load is represented by the square plate shown in Figure 13(a). The columns are attached to the roof in a region which is a non-design domain with a thickness of $h_c = 0.05$. The size of a column supporting the roof is $c = 1$ and its position on the roof is $b = 3$. The central layer has a thickness of $h_0 = 0.05$ and the top and bottom layers have a thickness of $h_1 = 0.05$. The thickness of the plate is $h = 0.1$. A central load of $P = -100$ is applied. The prescribed volume fraction is $V_{\text{frac}} = 30$ per cent. The optimum layout obtained is shown in Figure 13(b). The design variables used in this case are the widths w_1, w_2, and w_3 as illustrated in Figure 13(c). The results obtained during the sizing optimization phase are $w_1 = 0.050$, $w_2 = 0.866$ and $w_3 = 2.882$ which are in good agreement with the topology layouts. There is an improvement of approximately 60 per cent in the SE.

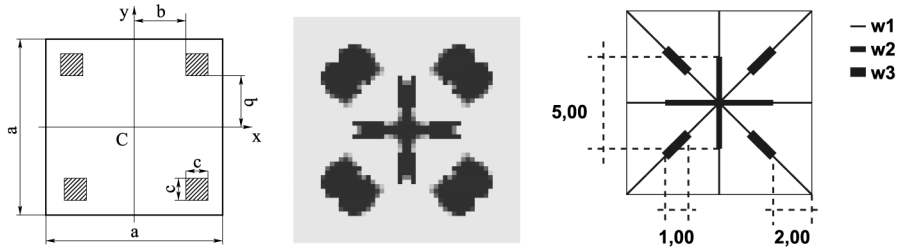

Figure 13.
Flat roof example

Notes: (a) geometry; (b) optimum topology and (c) optimum stiffeners distribution

8.4 EP shell

The first shell studied is an EP shell defined geometrically by the equation $z(x, y) = 0.57(x^2 + y^2)$. In the present the length of the shell is bounded by $[-1,1]$. The shell is subjected to a central point $P = -400$ and the whole edges are clamped. The material properties considered are: elastic modulus $E = 10,920$, Poisson's ratio $\nu = 0.3$. The central layer has a thickness of $h_0 = 0.05$ and the top and bottom layers have a combined thickness of $h_1 = 0.05$. The volume fraction considered here is $V_{\text{frac}} =$ 30 per cent. Figure 14(a) shows the emerging layout from TO. Two stiffening cross lines are incorporated into the shell. For each stiffener three different regions are assigned (Figure 14(b)). The widths w_1, w_2 and w_3 associated to region 1, 2 and 3 are optimized in the sizing optimization stage. The optimum values found are $w_1 = 0.005$, $w_2 = 0.0005$ and $w_3 = 0.1$. A 60 per cent improvement in the SE is obtained.

8.5 Cylindrical shell

A cylindrical shell subject to a central point load $P = -40\,\text{N}$ is now considered. The shell is clamped at four corners and the following material properties and dimensions are assumed: elastic modulus $E = 2.1 \times 10^8\,\text{N/m}^2$, Poisson's ratio $\nu = 0.3$, radius $R = 0.86\,\text{m}$, span $L = 1.0\,\text{m}$ and $ht_{sh} = 0.005\,\text{m}$. For the three-layer FE model, the central layer thickness is $h_0 = 0.002\,\text{m}$. The volume fraction considered is $V_{\text{frac}} =$ 35 per cent. Figure 15(a) presents the optimum layout obtained. From this the cylindrical shell appears to require a major stiffener along the straight line of the centre of the cylindrical shell and other minor regions of stiffening along two diagonal lines

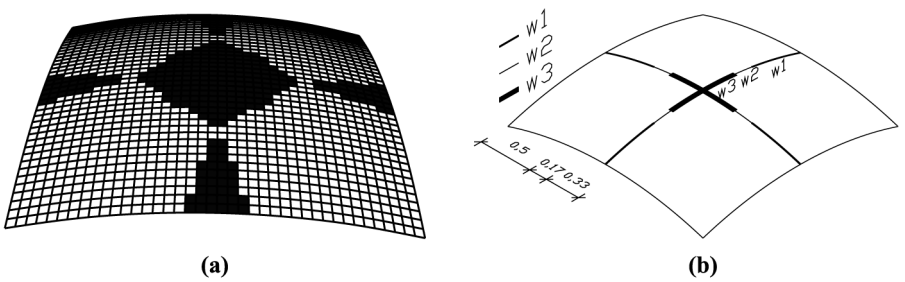

Figure 14.
EP shell example

Notes: (a) optimum topology and (b) optimum stiffeners distribution

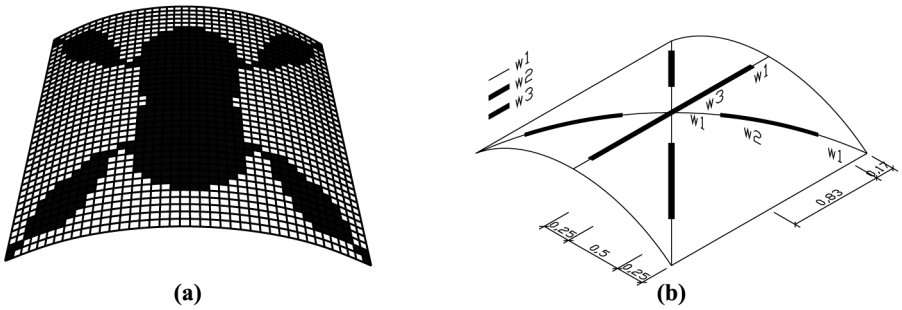

Figure 15.
Cylindrical shell example

Notes: (a) optimum topology and (b) optimum stiffeners distribution

crossing the shell. This is represented in Figure 15(b). Along these stiffeners three different regions which are related to three design variables w_1, w_2 and w_3 are defined. The results obtained in the sizing optimization stage are $w_1 = 0.50 \times 10^{-6}$, $w_2 = 0.40 \times 10^{-2}$ and $w_3 = 0.43 \times 10^{-2}$ and a total of 20 per cent improvement in the SE is obtained. It is important to mention here that the final value for w_1 is the lower bound value specified in the optimization. This is consistent with the topology layout presented.

As can be seen from these examples the step from the TO result presented as image to a stiffener layout and separation into individual design variables depends on the subjective interpretation of the user. Therefore different layouts might be obtained.

9. Conclusions

This work showed the use of different optimization strategies to obtain an optimal design for plates and shells. Both TO and SSO procedures were considered. These two optimization applications, as separate procedures produce new designs with a great improvement when compared to the initial designs. However, the combination of stiffening TO and sizing optimization using integrally stiffened shells appears as an even more attractive tool to be used. This was illustrated with several examples. This represents a novel approach to the design of optimally stiffened shells and overcomes the drawbacks of both TO and SSO procedures when applied individually. Furthermore, the unique use of integrally stiffened shell elements for optimization, unlike conventional shell stiffening optimization techniques provided a general and extremely flexible tool.

References

Afonso, S.M.B. (1995), "Shape optimization of Mindlin-Reissner shells under static and free vibration conditions", PhD thesis, Department of Civil Engineering, C/Ph/188/95, University of Wales, Swansea.

Afonso, S.M.B. and Antonino, G.C.R. (1998), "Generation of optimal stiffening layout for plates using a structural shape optimization procedure", paper presented at the IV World Congress on Computational Mechanics, Buenos Aires.

Afonso, S.M.B. and Antonino, G.C.R. (1999), "Analysis and optimum design of stiffened structures", paper presented at the XX Congresso Ibero Latino Americano de Métodos Computacionais em Engenharia, São Paulo.

Ahmad, S. (1969), "Curved finite elements in the analysis of solid shell and plate", PhD thesis, Department of Civil Engineering, C/Ph/7/69, University College of Swansea, Swansea.

Baumgartner, A., Harzheim, L. and Matteck, C. (1992), "SKO soft kill option. The biological way to find an optimum structure topology", *International Journal of Fatigue*, Vol. 14 No. 6, pp. 387-93.

Belblidia, F. (1999), "Fully integrated design optimization for plate structures FIDO-plates", PhD thesis, Department of Civil Engineering, C/Ph/231/99, University of Wales, Swansea.

Belblidia, F. and Bulman, S. (2002), "A hybrid topology optimization algorithm for static and vibrating shell structures", *International Journal for Numerical Methods in Engineering*, Vol. 54 No. 6, pp. 835-52.

Belblidia, F. and Hinton, E. (2002), "Fully integrated design optimization of plate structures", *Finite Elements in Analysis and Design*, Vol. 38, pp. 227-44.

Belblidia, F., Afonso, S.M.B., Hinton, E. and Antonino, G.C.R. (1999), "Integrated design optimization of stiffened plate structures", *Engineering Computations*, Vol. 16, pp. 934-51.

Belblidia, F., Afonso, S.M.B. and Sienz, J. (2001), "Comparison of single and three layered material models in the hybrid topology optimization of shell structures", *The third ASMO Engineering Design Optimization Conference*, *Harrogate, July*, pp. 41-7.

Bendsøe, M.P. and Kikuchi, N. (1988), "Generating optimal topologies in structural design using homogenization method", *Computer Methods in Applied Mechanics and Engineering*, Vol. 71, pp. 197-224.

Bendsøe, M.P. and Sigmund, O. (2003), *Topology Optimization: Theory, Methods and Applications*, Springer, Berlin.

Bulman, S. and Hinton, E. (1999), "Constrained adaptive topology optimization of engineering structures", *Design Optimization*, Vol. 1, pp. 19-439.

Cheng, K.T. and Olhoff, N. (1981), "An investigation concerning optimal design of solid elastic plates", *International Journal of Solids and Structures*, Vol. 17, pp. 305-23.

Chipalo, M., Bettess, P. and Bull, J.W. (1994), "A nine-node stress resultant integrally stiffened shell element", *The Second International Conference on Computational Structures Technology*, *Athens*, pp. 57-62.

Falco, S.A., Afonso, S.M.B. and Vaz, L.E. (2004), "Analysis and optimal design of variables thickness plates and shells under dynamic loads – I: finite element and sensitivity analysis, II: optimization", *Structural Optimization*, Vol. 27, pp. 189-209.

Gea, H.C. and Luo, J.H. (1999), "Automated optimal stiffener pattern design", *Mechanics of Structures and Machines*, Vol. 27, pp. 275-92.

Hassani, B. and Hinton, E. (1999), *Homogenization and Structural Topology Optimization*, Springer, London.

Huang, H.C. and Hinton, E. (1986), "A new nine-node degenerated shell element with enhanced membrane and shear interpolation", *International Journal for Numerical Methods in Engineering*, Vol. 22, pp. 73-92.

Lagaros, N.D., Fragiadakis, M. and Papadrakakis, M. (2004), "Optimum design of shell structures with stiffening beams", *AIAA Journal*, Vol. 1, pp. 175-84.

Luo, J.H. and Gea, H.C. (1998), "A systematic topology optimization approach for optimal stiffener design", *Structural Optimization*, Vol. 16, pp. 280-8.

Maute, K. and Ramm, E. (1997), "Adaptive topology optimization of shell structures", *AIAA Journal*, Vol. 35, pp. 1767-73.

Paley, M., Fuchs, M.B. and Miroshnik, E. (1996), "The aboudi micromechanical model for shape design of structures", *The Third International Conference on Computational Structures Technology*, *Budapest*, pp. 21-3.

Powell, M.J.D. (1978), "Algorithms for nonlinear constraints that use lagrangian functions", *Mathematical Programming*, Vol. 14, pp. 224-48.

Rao, N.V.R. (1992), "Computer aided analysis and optimisation of shell structures", PhD thesis, Department of Civil Engineering, C/Ph/160/92, University of Wales, Swansea.

Rozvany, G.I.N. (2000), "Problem classes, solution strategies and unified terminology of FE-based topology homogenization", *The NATO Advanced Research Workshop on Topology Homogenization of Structures and Composite Continua*, *Budapest*, pp. 19-35.

Rozvany, G.I.N., Zhou, M. and Biker, T. (1992), "Generalized shape optimization without homogenization", *Structural Optimization*, Vol. 4, pp. 250-2.

Sienz, J. (1994), "Integrated structural modelling, adaptive analysis and shape optimization", PhD thesis, Department of Civil Engineering, C/Ph/181/94, University of Wales, Swansea.

Soto, C. and Diaz, A. (1993), "On modeling of ribbed plates for shape optimization", *Structural Optimization*, Vol. 6, pp. 175-88.

Suzuki, K. and Kikuchi, N. (1991), "A homogenization method for shape and topology optimization", *Computer Methods in Applied Mechanics and Engineering*, Vol. 93, pp. 291-318.

Tenek, L.H. and Hagiwara, I. (1994), "Optimal rectangular plate and shallow shell topologies using thickness distribution or optimization", *Computer Methods in Applied Mechanics and Engineering*, Vol. 115, pp. 111-24.

Thompson, P.A. (1989), "Stiffened shell element development and application to perforated structures", PhD thesis, Newcastle University, Newcastle.

Xie, Y.M. and Steven, G.P. (1997), *Evolutionary Structural Optimization*, Springer, Berlin.

Zhou, M. and Rozvany, G.I.N. (1991), "The COC algorithm, part II: topological, geometrical and generalized shape optimization", *Computer Methods in Applied Mechanics and Engineering*, Vol. 89, pp. 309-36.

Zienkiewicz, O.C. and Taylor, R.L. (2000), *The Finite Element Method*, Vol. II, McGraw-Hill, New York, NY.